Design principle of heparanase inhibitors: a combined in vitro and in silico study

Yuzhao Zhang, Meijun Xiong, Zixin Chen, Gustavo Seabra, Jun Liu, Chenglong Li, and Lina Cui*

Department of Medicinal Chemistry, College of Pharmacy, UF Health Science Center, UF Health Cancer Center, University of Florida, Gainesville, FL 32610, USA

*Corresponding Author: Prof. Lina Cui (linacui@cop.ufl.edu)

Abstract

Heparanase (HPSE) is an enzyme responsible for the cleavage of heparan sulfate (HS) side chains from heparan sulfate proteoglycans (HSPGs). The enzymatic activity of HPSE contributes to ECM remodeling, regulates growth factors, and its overexpression has been implicated in various types of cancer and inflammation, making it a highly promising therapeutic target. In the last two decades, a number of HPSE inhibitors have been reported by labs worldwide, with most of them belonging to the saccharide-based category. So far, few of the small molecule HPSE inhibitors have progressed into clinical trials and none has gained approval by regulatory agencies, leaving a blank in HPSE drug discovery. Here we present the discovery of a novel HPSE small molecule inhibitor by high-throughput screening using an ultrasensitive HPSE enzymatic activity detecting probe developed in our lab and provide the mechanisms of action behind the HPSE inhibition of the small molecule. By doing a series of molecular dynamics (MD) simulations, we discovered the binding profiles on the derivatives of the lead compound. We summarized the essential structural features of the lead compound to provide insights into the design of future HPSE small molecule inhibitors.

Keywords

Heparanase inhibitor; molecular dynamics simulation; molecular modeling; drug discovery

Introduction

Heparanase (HPSE), an endo-β-D-glucuronidase of the glycoside hydrolase 79 (GH79) family, modulates the extracellular matrix (ECM) functionality and stability by cleaving glycosaminoglycan heparan sulfate (HS) side chains from heparan sulfate proteoglycans (HSPGs) [1,2,3]. HSPGs are an fundamental component of ECM, consisting of core proteins conjugated to one or more HS units [4,5]. As an essential component of ECM and cell surface, HSPGs support ECM's stability and integrity, interact with the cell surface and ECM with HS side chains, and participate in various signaling pathways [6]. The HS units bind to HSPGs through covalent O-link and play an important role in

realizing HSPGs' functions. HPSE is the only known enzyme that cleaves the internal glycosidic bond between a glucuronic acid (GlcUA) residue and an N-sulfoglucosamine (GlcN(NS)) residue bearing a 3-O-sulfo or a 6-O-sulfo group [7]. HS is a series of repeating disaccharides consisting of specific patterns of glucuronic acid and D-glucosamine that have been N-sulfated or N-acetylated, allowing HPSE to recognize and cleave. By releasing active carbohydrate framents by cleaving HS, HPSE changes the functionality of HSPGs, leads to ECM remodeling, and impacts downstream pathways activated by free HS. HPSE plays an essential role in cancer development, and has been suggested to be a potent driver of all hallmarks of cancers [8]. The elevated activity of HPSE is also reported in various inflammatory diseases, autoimmune disorders [9]. Pathologically, the overexpression of HPSE is associated with metastasis, angiogenesis, increased tumor size, and poor prognosis [2,10]. Additionally, HPSE is involved in diabetes [11], bone necrosis [12], fibrosis [13,14], and Alzheimer's disease [15]. Given its critical role in diseases, HPSE is considered a promising drug target [16].

Structurally, HPSE is a non-covalently linked heterodimer consisting of an 8 kDa N-terminal fragment and a 50 kDa C-terminal fragment [17]. HPSE is first produced as a pro-enzyme named pro-HPSE, which is further matured to become active enzyme within lysosomes [3]. GLU225 and GLU343 are the two catalytic residues located in the HPSE catalytic site that serve as a proton donor and a nucleophile lying in a 10 Å cleft [18]. This catalytic cleft is one of the most important sites where inhibition could happen. Heparin binding domain-2 (HBD-2), which consists of residues GLN270-LYS280 of HPSE, is also suggested to be a druggable region [16]. The glycine loop (GLY349-GLY351) is close to HPSE binding pocket and is important for substrate recognition (**Figure 1**). In addition, any residue that takes part in substrate binding of HPSE can be considered a good interaction spot.

The existing potent HPSE inhibitors are mostly derivatives of oligosaccharides or polysaccharides that mimic the natural HPSE inhibitor heparin. However, such mimetics are less favored due to their large molecular weight, highly hydrophilic and polyanionic nature. Also, HPSE is present in tissue both extracellularly and intracellularly, including within the nucleus, which makes the target unreachable by the negatively charged inhibitors. Up to date, none of HPSE inhibitors have been approved as drugs, with five (**PI-88** [19], **PG545** [20], **SST0001** [21], **M-402** [22], and **sulodexide** [23]) that have entered clinical trials are all saccharide-based. Except for oligo and polysaccharides, small molecule, nucleic acid, and antibody-based therapeutics targeting HPSE are also reported. Small molecule HPSE inhibitor discovery has been undergoing for decades, with various scaffolds reported [24,25,26,27,28,29,30]. To date, none of the designed small molecule drugs entered clinical trials, leaving a gap in the development of HPSE small molecule inhibitors. Traditional medicinal chemistry methods have been widely applied in HPSE inhibitors discovery, with only a few computational methods incorporated HPSE inhibitor design studies reported. There are several studies incorporating high throughput screening [24,25,29,31,30,32], pharmacophore modeling [33,34,35], and molecular dynamics (MD) simulation [35,36], from which some promising HPSE small molecule inhibitors have are discovered or inhibitory mechanism of existing HPSE inhibitors are revealed. Herein, we report a case study combining in vitro and in silico methods,

including high-throughput screening, organic chemistry synthesis, molecular docking, and MD simulation, to reveal TC LPA5 4 as an HPSE inhibitor and provide design ideas on the novel ligand-based HPSE inhibitor design.

Results and Discussion

Discovery of TC LPA5 4 as a novel HPSE inhibitor and the ligand-based design of a new small molecule

In our previous study, we successfully discovered a novel HPSE inhibitor in a high-throughput screening study using the ultrasensitive HPSE activity detecting fluorogenic probe **HADP** [31]. The selected small molecule, TC LPA5 4 (**Figure 2A**), is a known LPA5 selective receptor antagonist (IC_{50}: 0.8 μM) [37,38]. The high-throughput screening result revealed that TC LPA5 4 exhibited promising HPSE inhibitory activity (IC_{50}: 10 μM, **Figure 2B**) and was chosen as the lead compound. In the initial molecular docking study, we discovered a potential binding mode between TC LPA5 4 and HPSE as shown in **Figure 2C**. Specifically, the carboxylic acid pyrazole ring formed polar interactions with LYS159 and ARG303, while the methoxy group formed a hydrogen bonding with THR97. Although we did not observe any interaction of HPSE with the chloride phenyl ring or the hexane ring, we hypothesized that the overall shape of the small molecule and the planar angle formed by the two phenyl rings with the pyrazole ring were crucial for the HPSE inhibitory activity. To optimize the structure of TC LPA5 4, we retained the overall structure and used carboxylic pyrazole as the core while adding polar groups on the methoxy phenyl group to yield a 2-aminophenol ring. We also changed the hexane ring to a pyrazole ring in the hopes of forming interactions with the polar residues ARG272 and GLN270, which are close to the lead compound based on the preliminary computational study. The resulting ligand-based designed small molecule, **MX4-62**, was synthesized as shown in **Figure 3A**. Unfortunately, **MX4-62** did not exhibit any HPSE inhibitory effect (**Figure 3B**), suggesting that further optimization using more sophisticated computational tools is necessary.

HPSE crystal structures comparison and identification of frequent interacting residues

To identify the critical interactions involved in HPSE-substrate or HPSE-inhibitor binding, we conducted a structure analysis of the HPSE binding pocket. In HPSE HS cleavage activity, GLU225 is a proton donor that protonates the O-linkage between the disaccharide units, then GLU343 acts as a nucleophile to attack the protonated linkage and accomplishes the cleavage. The two catalytic residues are the crucial site for inhibiting in the ideal situation. During the cleavage, the endogenous substrate also interacts with ASP62, ASN64, THR97, ASN224, GLN270, ARG272, GLY349, GLY350, GLY389, and TYR391. These interactions can be observed in HPSE co-crystalized structure 5E9C, which is co-crystalized with a heparin-derived tetrasaccharide (dp4) as shown in **Figure 4A** [39]. To compare the substrate binding and the inhibitor binding

modes with HPSE, we analyzed the interactions established in other HPSE crystal structures, including 5E98, 7PR7, 7PR8, and 7PRT [40], as shown in **Figure 4B-4E**. The binding conformations of the small molecules with the HPSE structure are shown in **SI, Figure S1**. Since 7PR7, 7PR8, and 7PRT are all co-crystalized with a small molecule inhibitor, the ligand-protein interactions provide a basic view for later inhibitor design. In summary, THR97, ASN224, GLU343, GLY349, GLY350, and TYR391 are essential residues in both substrate binding and inhibitor binding. Meanwhile, we should also pay attention to the interactions with ASP62, ASN64, GLN270, GLN272, and GLY389, as these interactions are constantly observed in substrate binding, which is another effective approach to inhibit HPSE activity by competing the substrate.

Reveal of lead-HPSE binding modes by MD simulation

We conducted a 500 ns MD simulation of the HPSE-lead complex and discovered three stable TC LPA5 4 binding conformations (**SI, Figure S2**), two of which explain the inhibitory mechanism of the small molecule. The third conformation had the carboxylic acid group pointing out of the binding pocket, which we deemed to lose useful interactions. The inhibition of a small molecule inhibitor like TC LPA5 4 is most straightforwardly brought about by its interactions with the catalytic residues GLU225 and GLU343 [41]. TC LPA5 4 also formed interactions with GLN270 and ARG272, two residues reside in another potential inhibitory domain HBD-2 (GLN270-LYS280) . Additionally, we identified TYR298, TYR348, and LYS231 as characteristic binding residues that stabilize TC LPA5 4 in the binding pocket. The 500 ns simulation revealed various types of interactions of TC LPA5 4, including hydrogen bond, ionic interaction, water bridge, and hydrophobic interaction with multiple other residues. The interaction heatmap **Figure 5A** and categorized interaction heatmaps are shown in **SI, Figure S3.** The time-combined residue interaction frequency is shown in **SI, Figure S4**).

The first binding mode sustained for the initial 100 ns of the MD, and the binding map is shown in **Figure 5B**. In this conformation, TC LPA5 4 pyrazole carboxylic acid ring 1 established hydrogen bonds with ASN224, GLU343, and THR97, and ionic interaction with LYS232. In the second conformation, the carboxylic acid group of TC LPA5 4 formed high frequency hydrogen bonding with GLU225, water bridges with GLU343, and occasional ionic interaction with LYS231. The interactions with TYR298 and TYR348, including hydrogen bond and water bridges, stabilized this conformation. Additionally, the molecule's methoxy phenyl ring 2 interacted with GLN270 by forming hydrogen bond or water bridges. This conformation was maintained for approximately 300 ns. Apart from the frequent interactions with GLU225, GLU343, TYR298, and TYR348, we observed the molecule's interactions with THR97, ASN224, GLN270, which drew our attention.

MX-62 dynamic behavior in HPSE binding pocket

In the 500 ns MD simulation of the HPSE-**MX4-62** complex, we started with a similar conformation to the lead compound's HPSE inhibiting conformation, with the carboxylic acid forming water bridges with GLU225 and hydrogen bonds with GLN270 and

LYS231. **MX4-62** was also close to TYR348, which stabilized the binding conformation of the lead compound through hydrophobic interactions (**Figure 6A**). However, during the initial 5 ns of the simulation, the flexible polar side chain of ARG303 interfered with aminophenol ring 2 and caused **MX4-62** to move away from the catalytic cleft by forming multiple interactions with the alcohol group on ring 2 and the aromatic system. This interaction allowed ring 2 to reach ASN390, which served as an anchor by forming hydrogen bonds with the aminophenol group of MX4-62, while ring 1 continued to interact with LYS231 (**Figure 6B**). As **MX4-62** was no longer able to fit in the large opening of the binding pocket, it started to search for other interactions. During the next 10 ns of simulation, the binding conformation of the small molecule continued to change due to the interactions with ASN390. The molecule moved to the edge of the binding pocket and formed a new ionic interaction with LYS98 and a hydrogen bond with TYR391. Additionally, ASP62 formed frequent water bridges with the carboxylic acid, while the aminophenol ring 2 continued to anchor **MX4-62** to other residues such as ARG303 and ALA388. Despite the polar residues' interactions with **MX4-62**, the carboxylic pyrazole core was further extracted from the catalytic cleft. So far, **MX4-62** is on the edge of the binding pocket and without any interaction formed with the catalytic cleft (10 ns to 20 ns, **Figure 6C**). Finally, in the remaining MD simulation, **MX4-62** flew away from the HPSE binding pocket, with no interaction formed with the potential inhibiting residues. Therefore, we conclude that the aminophenol group played a crucial role in forming interactions with ARG303 and ARG390, leading to the small molecule to move away from the binding site.

TC LPA5 4 SAR study based on MD simulations

We further conducted a computational SAR study based on MD simulations to investigate the TC LPA5 4 and its relationship with HPSE inhibition. To assess the importance of the four-ring structure and substitutions in binding, we designed nine TC LPA5 4 derivatives (**Figure 7A**, **8A**, **9A**) and subjected each system to a 200 ns MD simulation. We categorized the nine molecules into three classes based on their structural features and modifications. The first class kept the four rings intact, only making modifications to chloride and methoxy groups. The second class, with the ring 4 removed to investigate its role in receptor binding, also had modifications on chloride and methoxy groups to further investigate the two substitution groups. The third class had the left handle (ring 3 and ring 4) removed to investigate the role of overall shape of the small molecule in binding. To achieve better comparison, all the system were built based on TC LPA5 4 MD starting point. During the simulations, we recorded the interactions and classified them into four types: hydrogen bonding, water bridges, ionic interaction, and hydrophobic interaction. The summary of overall interaction for each system is shown in **Figure 7-9**. Our study revealed that the four-ring system of the TC LPA5 4 is crucial for inhibitory activity. Removing the hexane ring or the hexane-chloride ring resulted in the loss of the GLU225 and GLU343 interactions. In class **1** molecules, we observed that the methoxy group increased contact frequency with GLN270, LYS231, and GLU225, while the chloride group increased interaction frequency with GLY349 and GLY350. Removing both substituents resulted in fewer pi-pi interactions

with TYR298. Although the chloride group was generally less important than the methoxy group in class **1** molecules, the removal of both substituents resulted in fewer interactions (**Figure 7B-7E**). The class **2** molecules showed a binding profile compared with the parallel molecules from class **1** but with less interaction frequency (**Figure 8B-8E**), suggesting that ring 4 contributed to the binding intensity through space-occupying. In contrast, the study on class 3 molecules revealed that the ring1-ring 2-core of the lead compound is crucial for the basic binding, and any design should not be smaller than **3a** (**Figure 9B-9C**). Specifically, **3a** managed to stay in the pocket during the simulation due to the methoxy group's ability to occupy space and provide useful interactions, while compound **3b** flew out of the pocket due to poor fitting. In summary, the first part of computational SAR study provides insights into the importance of the four-ring system and the substitution groups in the TC LPA5 4 structure for HPSE inhibition. These finding can be sued to guide the further HPSE inhibitor development.

We conducted an additional series of 200 ns MD simulations to further study the substitution groups and positions on TC LPA5 4. We designed class **4** molecules (**Figure 10A**) to study the substitution position and type on ring 2. Firstly, we changed the methoxy substitution position on ring 2 from meta to ortho and para (**4b** and **4c**). Based on the interaction profile, we exclude the ortho-substitution from further study, as it impaired the overall interaction (**Figure 10B**). However, the p-OMe **4b** (**Figure 10C**) showed a similar binding profile to the lead compound but exhibited stronger interactions with GLU225 and TYR298 and weaker interactions with GLN270, indicating that the para-substitution on ring 2 could be a good optimization position. Next, we investigated hydrogen bond donor (HBD) substitution group by using **4c** (**Figure 10D**), with the methoxy group changed to a hydroxyl group. However, **4c** showed much fewer interactions with GLU225 and lost almost all interactions with GLU343. The m-F substituted **4d** (**Figure 10E**) showed weaker interactions and loss of interaction diversity, suggesting that the size of the substitution group was essential in the SAR. Overall, we concluded that a para-substituted hydrogen bond acceptor (HBA) no smaller than fluorine might be a suitable option to optimize ring 2.

Next, we investigated ring 3 using class **5** molecules (**Figure 11A**). We started with **5a,** as shown in **Figure 11B**, with the meta-substituted chloride replaced with the ortho-position. **5a** exhibited a much weaker interaction profile, likely because ring 3 of **5a** was prevented from rotating, resulting in a change in the overall conformation of the molecule. We then replaced the m-Cl with m-Br substituted to yield **5b** (**Figure 11C)** but found that the larger halide group did not improve interactions with key residue. However, we observed multiple interactions improvements with m-F (**5c, Figure 11D**) or m-OMe (**5d, Figure 11E**), suggesting that HBA substitutions on ring 3 were beneficial. Moreover, **5c** and **5d** shared very similar binding profiles. We also tried a methyl substitution but observed weaker binding. Thus, we concluded that m-substitution benefited the overall interaction profile, with fluorine and methoxy substitution options worth exploring.

Lastly, we examined the type and size of ring 4 and the potential optimization strategies using class **6** molecules (**Figure 12A**). We first replaced hexane to benzene (**6a, Figure**

12B) and found that **6a** had a very different binding profile from TC LPA5 4. This finding confirmed that the non-aromatic substitutions were important to the overall binding profile. We then added a para-substitution on ring 4 to yield molecules **6b**, **6c**, and **6d** (**Figure 12C-12E**). We found that bulkier substitution was preferred at the para-position, prompting us to design **6e** (**Figure 12F**). **6e** showed a cleaner binding profile and improved interactions with GLU225 and LYS231.Based on these MD simulations and data analysis, we summarized the SAR and optimization strategy for TC LPA5 4 in **Figure 13**.

Materials and Methods

Synthesis of MX4-62

Figure 3A, illustrates the overall synthetic route of **MX4-62**. To provide a comprehensive understanding of the synthesis, the stepwise protocol and related spectra have been deposited in **SI**. The synthesis commenced by an addition reaction of pyrazole with 4'-Iodoacetophenone, which resulted in the compound **MX4-1** as a yellow solid. Subsequently, compound **MX4-1** underwent an S_N2 reaction with dimethyl oxalate, producing compound **MX4-5**. The next step involved a Knorr reaction of **MX4-5** with phenyl butanoate, yielding **MX4-72.** The nitro group of compound **MX4-72** was reduced in the subsequent step, resulting in the formation of **MX4-61**. Finally, hydrolysis of the methyl ester group of **MX4-61** yielded the final product, **MX4-62**.

Heparanase inhibition assay

The recombinant human active heparanase used in the bioassay was purchased from R&D systems (lot number: DCEM0320071). To Eppendorf tubes containing 40 µL 40 mM NaOAc (pH = 5.0), 5 µL of 0.005 µg/µL heparanase was added, followed by 5 µL of various concentrations (0.001, 0.01, 0.1, 1.0, 10, 100, 1000 µM) of the compounds (TC LPA5 4, **MX4-62**). The tubes were incubated at 37 ºC for 1 h. After the incubation period, 5 µL of HADP probe (50 µM) was added to each tube, and the tubes were further incubated at 37 °C for 4 hours. The plate reader was configured to measure florescence with λex = 365 nm and λem = 455 nm. The relative fluorescent intensity was plotted as a function of logarithm of compound concentrations.

Complex preparation and molecular docking

To conduct the modeling and molecular docking study, we obtained the crystal structure of human HPSE (PDBID: 5E98) [39] from Protein Data Bank [42] for the following modeling and docking study. The protein underwent a series of cleaning procedures to remove water molecules and ions outside the binding pocket. The protein preparation wizard [43] suite was then applied to further refine the protein's structure, including resolving alternative residue positions and minimizing the complex energy. GLU225 was protonated to restore its catalytic function in active form of HPSE. A local minimization

was performed to optimize the binding pocket, followed by generating a grid box using the OPLS2005 force field, with an inner box size of 10 Å x 10 Å x 10 Å and an outer box of 25 Å x 25 Å x 25 Å, based on the substrate binding site of 5E98. The small ligands used in the study were prepared using Ligand Preparation module [44] in Schrödinger Maestro, and their pKa values and protonation states were determined under pH 6.5 ± 0.5 using Epik [45]. We used Glide XP precision [46] to generate complexes of HPSE and small ligands. The resulting complex structures were manually selected for the MD simulation study.

Molecular dynamics simulations

To conduct the MD simulations, we used the Schrödinger Desmond [47]. The prepared complexes from the previous modeling were immersed in an orthorhombic water box using SPC water molecules with a minimum distance of 10 angstroms to the edges of the HPSE-ligand complex. Chloride ions were added to neutralize the system. As the result of preparation, resulting in a complete system containing around 14000 SPC water molecules, 17 Cl^- ions, and one HPSE-ligand complex, comprising around 42000 atoms. We then performed a 100 ps minimization to relax the system. For the MD simulations, we used the NPT ensemble class, set the simulation temperature to 300 K (Nose-Hoover chain), and the pressure was set to 1.01325 bar (Martyna-Tbias-Klein). The simulations were conducted following OPLS4 force field [48] incorporated in Desmond Molecular Dynamic module. We simulated the TC LPA5 4 and **MX4-62** systems for 500 ns, with 2500 frames recorded evenly in 200 ps stepwise during the MD production phase. For the complexes built for the SAR study, we simulated for 200 ns, with 1000 frames recorded evenly in 200 ps stepwise during the MD production phase. We used simulation Interactions Diagram (SID) module to perform post-MD analysis, extracting specific interaction information for further analysis based on SID results.

Conclusion

In this study, we have employed a multidisciplinary approach combining high-throughput screening (HTS), organic synthesis, molecular modeling, and molecular dynamics (MD) simulations to investigate TC LPA5 4, a promising inhibitor of heparanase (HPSE). Our analysis of co-crystalized complexes of HPSE with small molecules allowed us to identify a list of essential residues in HPSE inhibitor design, including catalytic residues GLU225 and GLU343, as well as other interacting residues. We then revealed an unfavorable binding conformation of TC LPA5 4 with HPSE that should be excluded in the future design by providing a design based on that binding conformation. Based on the 500 ns MD simulation of the lead-HPSE complex, we proposed two binding conformations for TC LPA5 4. Additionally, we summarized the binding heatmap of TC LPA5 4 with the HPSE binding pocket and concluded the dynamic behavior of the lead compound and potential inhibitory mechanisms. Further MD simulations of smaller TC LPA5 4 derivatives allowed us to identify the minimal core of the lead and the importance of the four-ring structure in overall binding, as well as the importance of the

substitutes on TC LPA5 4. We then performed another two series of MD simulations on additional TC LPA5 4 derivatives, investigating the effects of substitution type and position, as well as the space-occupying effect of the non-aromatic ring on binding. Based on these results, we developed a structure-activity relationship theory and proposed potential modifications for future lead optimization. Overall, our study provides insights into the design of small-molecule inhibitors, presents a promising candidate for further optimization, and contributes to the understanding of inhibitory mechanisms of HPSE.

Key Points

- In this case study, TC LPA5 4 was identified as a novel HPSE inhibitor lead in a high-throughput screening assay.
- A novel small molecule, **MX4-62**, was synthesized and tested for HPSE inhibitory activity.
- Using computational tools, we found two potential HPSE inhibitory conformations of TC LPA5 4 that may explain the inhibitory mechanism.
- We explored the options for TC LPA5 4 optimizations by simulating a series of derivatives based on the lead-HPSE model.
- SAR is summarized for TC LPA5 4 in HPSE inhibition.

Supplementary Information

Figure S1 shows the interaction information of 5 small molecules co-crystalized with HPSE.
Figure S2 shows the RMSD of TC LPA5 4 in 500 ns MD simulation with HPSE and the RMSD of protein backbone in 500 ns MD simulation.
Figure S3 shows the binding heatmaps of TC LPA5 4 with HPSE categorized in hydrogen binding, salt bridges, ionic interaction, and hydrophobic interaction.
Figure S4 shows the binding frequency summarized in residues of TC LPA5 4 with HPSE in 500 MD simulation.
Figure S5 shows the RMSD of molecules **1a**-**1c**, **2a**-**2c**, **3a**-**3b** with HPSE in 200 ns MD simulations.
Figure S6 shows the RMSD of molecules **4a**-**4d**, **5a**-**5e**, **6a**-**6e** with HPSE in 200 ns MD simulations.

Acknowledgements

This work is supported by research grants to Prof. L. Cui from the National Institute of General Medical Sciences of National Institutes of Health (Maximizing Investigators' Research Award for Early Stage Investigators, R35GM124963), and the University of Florida (UF Startup Fund).

Conflict of Interests

The authors declare no conflict of interests.

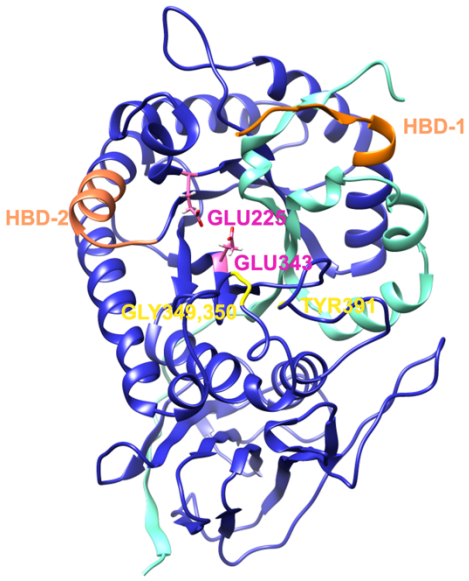

Figure 1. The structural and functional domains of human heparanase (HPSE) (PDB ID: 5E98). The 8 kDa chain-A is shown in cyan. The 50 kDa chain B is shown in blue. The enzymatic site is shown in pink, including proton donor GLU225 and nucleophile GLU343 that catalyze the cleavage of HS from HSPG. The glycine loop (GLY349, GLY350, and GLY350) of HPSE is shown in yellow. Substrate recognition residue TYR391 in yellow is in the proximity of the glycine loop. The two heparin binding domains (HBD) are shown in orange. HBD-1: LYS159-VAL170; HBD-2: GLN270-LYS280.

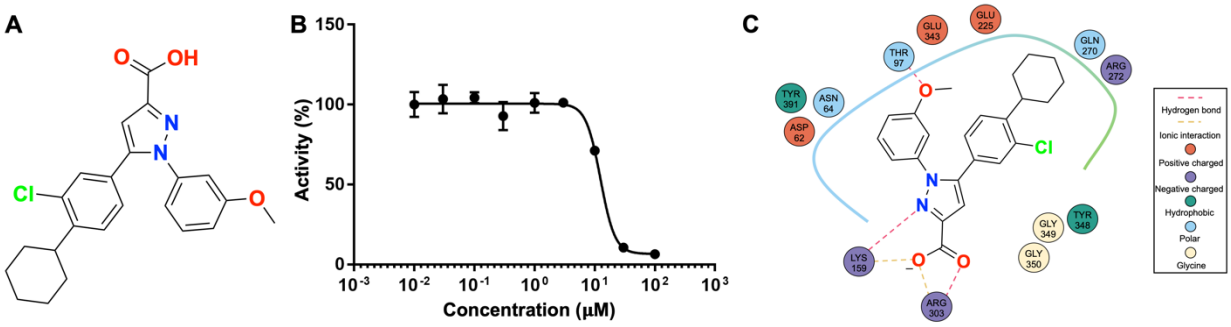

Figure 2. (**A**) The structure of the lead compound, TC LPA5 4, discovered in our lab via wet-lab HTS. (**B**) The HPSE inhibitory activity of TC LPA5 4 (figure adapted from reference [31]). HPSE inhibitory IC_{50}: 10 μM. (**C**) The binding conformation of TC LPA5 4 with HPSE in a molecular docking study.

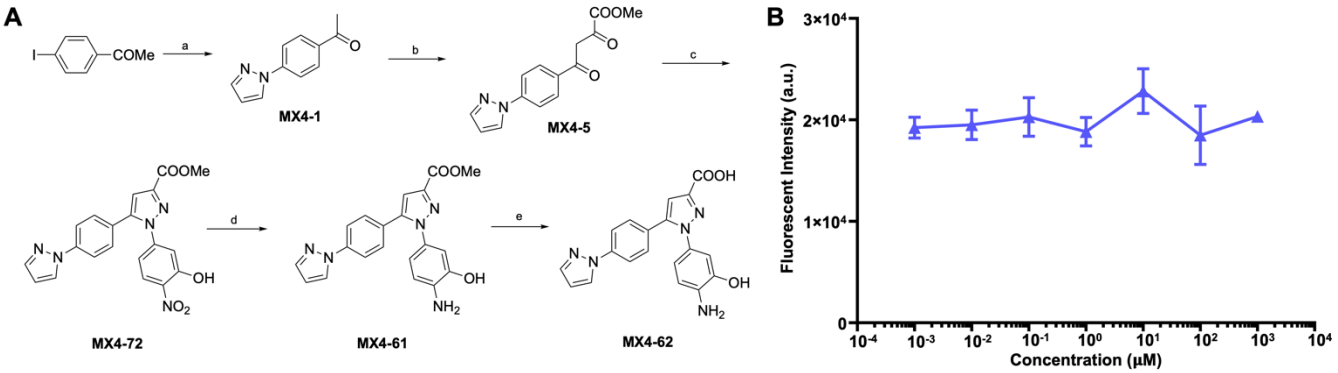

Figure 3. (**A**) The synthetic route of **MX4-62**. a: pyrazole; 10 mol% Cu_2O; 2.0 equiv Cs_2CO_3; DMF; 100°C; 24h. b: dimethyl oxalate; 1.3 equiv ^{t}BuOK; THF; 0°C to rt under Argon; overnight. c: 5-hydrazineyl-2-nitrophenol; 0.1M HCl; MeOH; 50°C; 24 h. d: 20% w/w Pd/C; H_2 balloon. e: pH = 12-13; THF/H2O (1:1); rt; 12 h. (**B**) Heparanase inhibition assay of **MX4-62.**

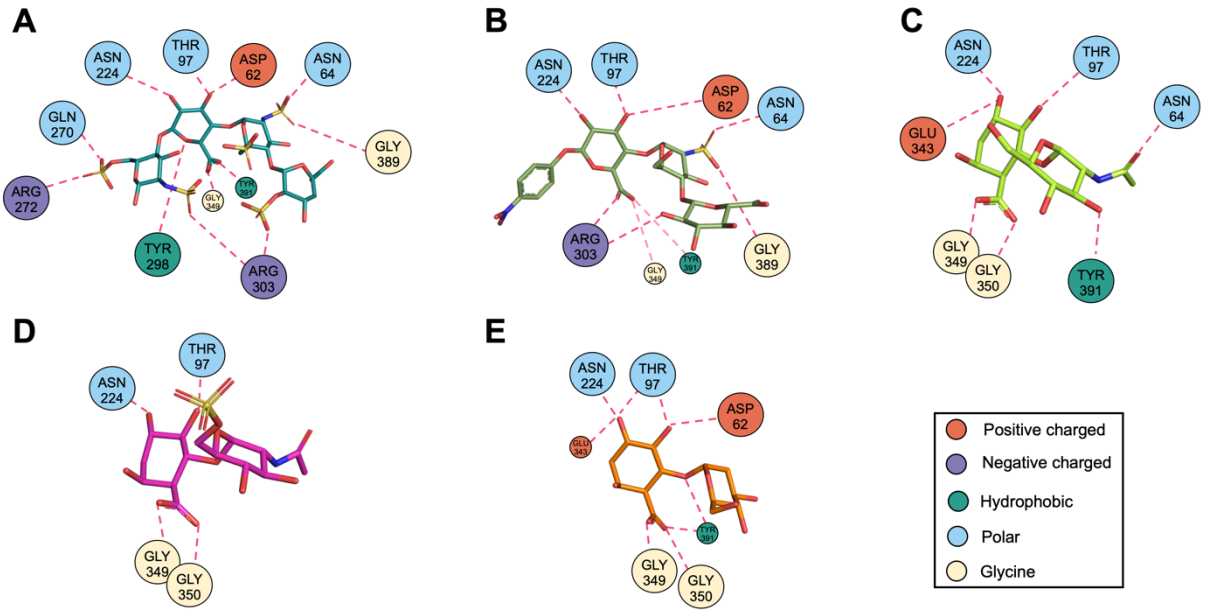

Figure 4. The interaction maps of (**A**) HPSE with **dp4** (PDB ID: 5E9C). (**B**) HPSE with **M04S02a** (PDB ID: 5E98). (**C**) HPSE with **VL166** (PDB ID: 7PR7). (**D**) HPSE with **GR109** (PDB ID: 7PR8). (**E**) HPSE with **CB678** (PDB ID: 7PRT).

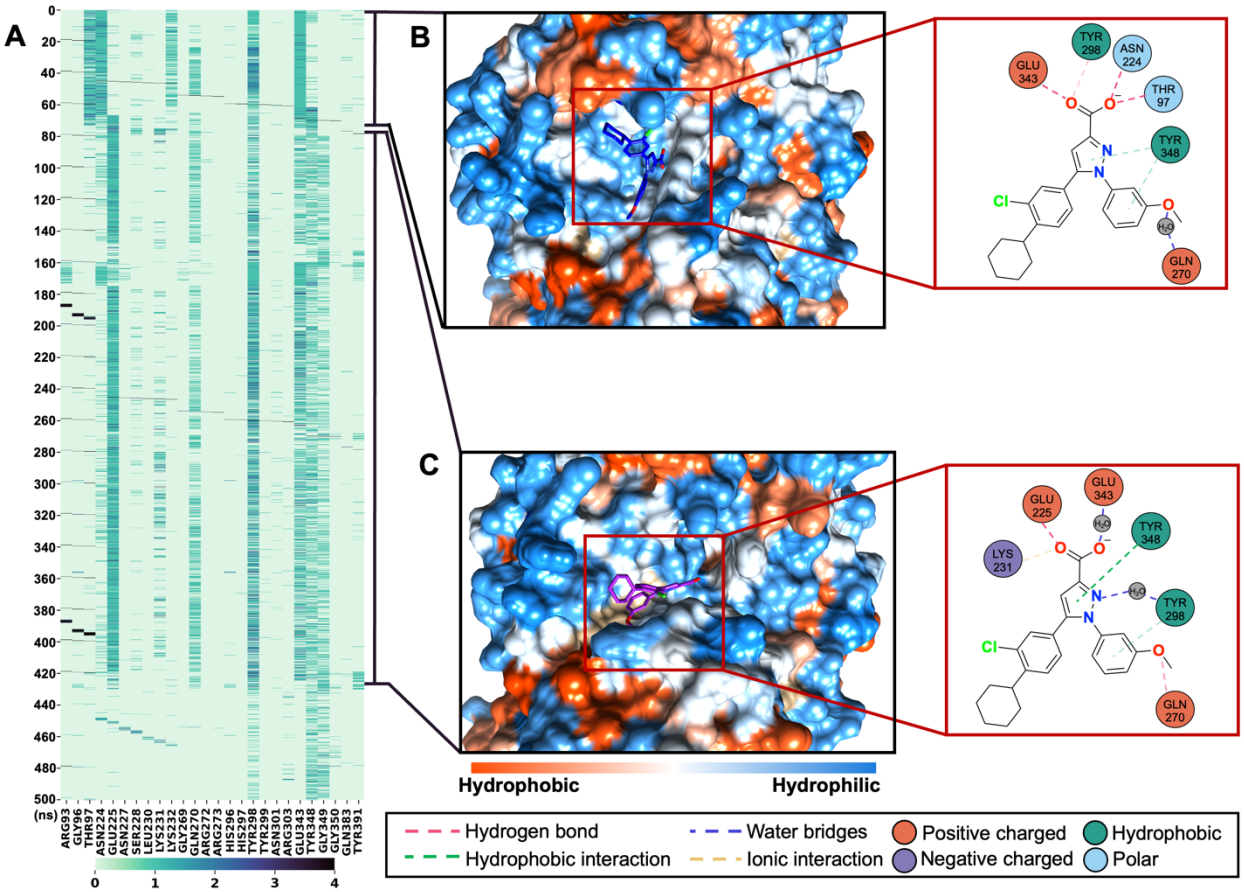

Figure 5. Binding conformations of TC LPA5 4 with HPSE identified from the 2500 frames sampled during the 500 ns molecular dynamics simulation. (**A**) Frequency heatmap of HPSE residues interacting with TC LPA5 4. (**B**) Conformation 1 and its detailed interaction with the receptor. (**C**) Conformation 2 and its detailed interactions with the receptor.

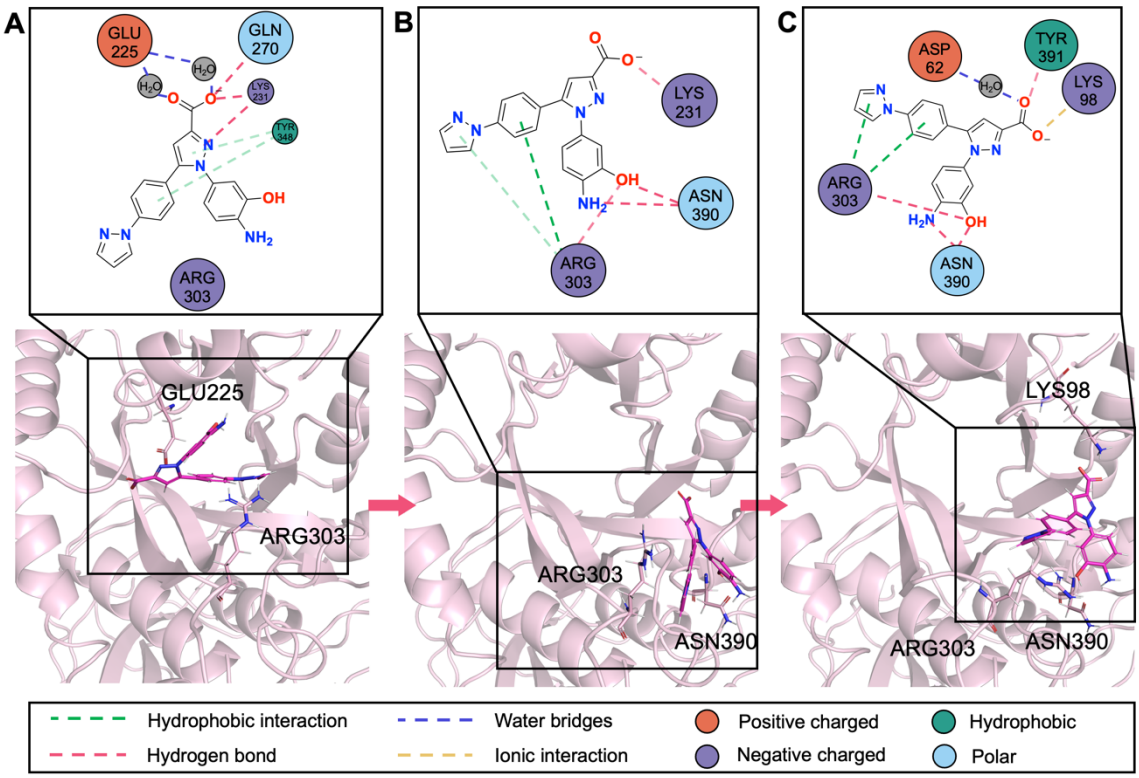

Figure 6. The dynamic behavior of **MX4-62** in HPSE binding pocket. (**A**) The first 5 ns interaction summary of **MX4-62** with HPSE. (**B**) The interaction summary of **MX4-62** with HPSE from 5 ns to10 ns. (**C**) The interaction summary of **MX4-62** with HPSE from 10 ns to 20 ns.

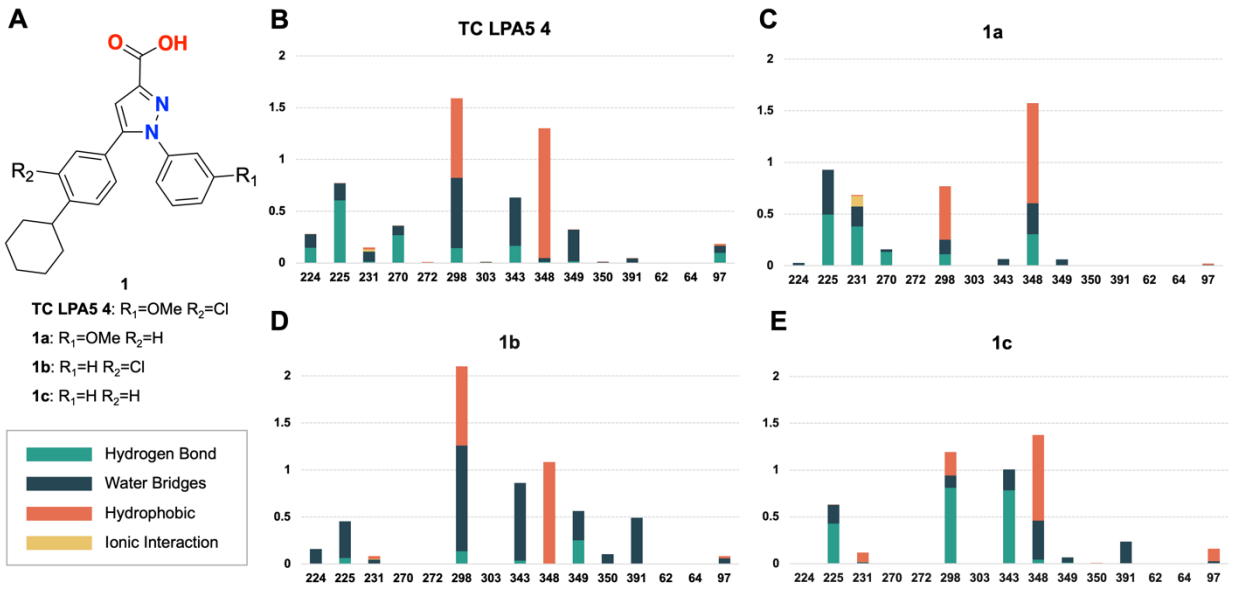

Figure 7. The binding profiles of class **1** molecules with heparanase (HPSE). The interactions are categorized in four types: hydrogen bond, water bridges, hydrophobic interaction, and ionic interaction. X axis: HPSE residue information; y axis: interaction frequency of the small molecule with the residue. (**A**) Class **1** molecule structures. (**B**) TC LPA5 4 and the interaction frequency in 500 ns molecular dynamics (MD) simulation. (**C**) **1a** and the interaction frequency in 200 ns MD simulation. (**D**) **1b** and the interaction frequency in 200 ns MD simulation. (**E**) **1c** and the interaction frequency in 200 ns MD simulation.

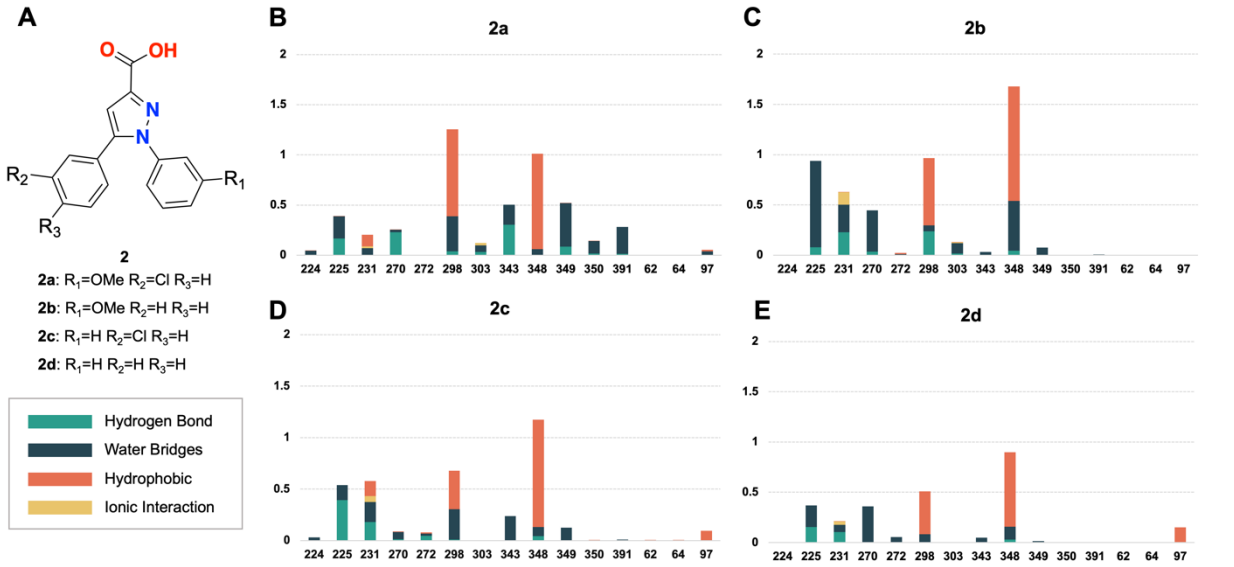

Figure 8. The binding profiles of class **2** molecules with heparanase (HPSE). The interactions are categorized in four types: hydrogen bond, water bridges, hydrophobic interaction, and ionic interaction. X axis: HPSE residue information; y axis: interaction frequency of the small molecule with the residue. (**A**) Class **2** molecule structures. (**B**) **2a** and the interaction profile with heparanase during 200 ns molecular dynamics (MD) simulation. (**C**) **2b** and the interaction profile with HPSE during 200 ns MD simulation. (**D**) **2c** and the interaction profile with HPSE during 200 ns MD simulation. (**E**) **2d** and the interaction profile with HPSE during 200 ns MD simulation.

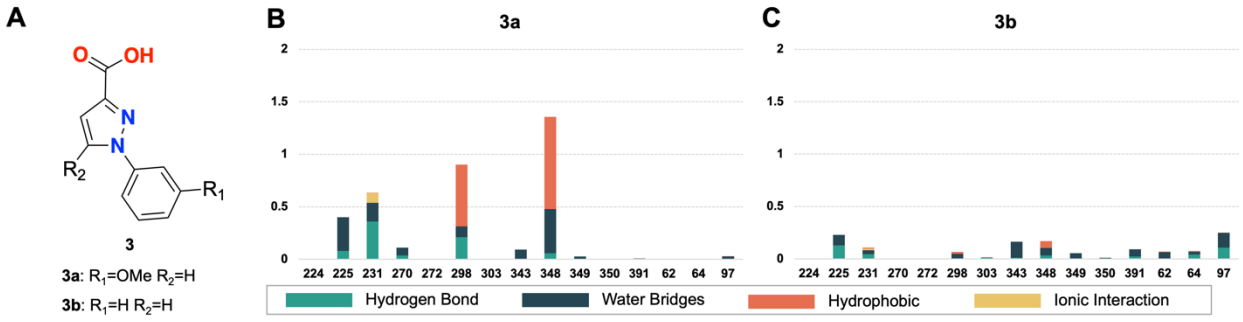

Figure 9. The binding profiles of class **3** molecules with heparanase (HPSE). The interactions are categorized in four types: hydrogen bond, water bridges, hydrophobic interaction, and ionic interaction. X axis: HPSE residue information; y axis: interaction frequency of the small molecule with the residue. (**A**) Class **3** molecule structures. (**B**) **3a** and the interaction frequency with HPSE during 200 ns molecular dynamics (MD) simulation. (**C**) **3b** and the interaction frequency with HPSE during 200 ns MD simulation.

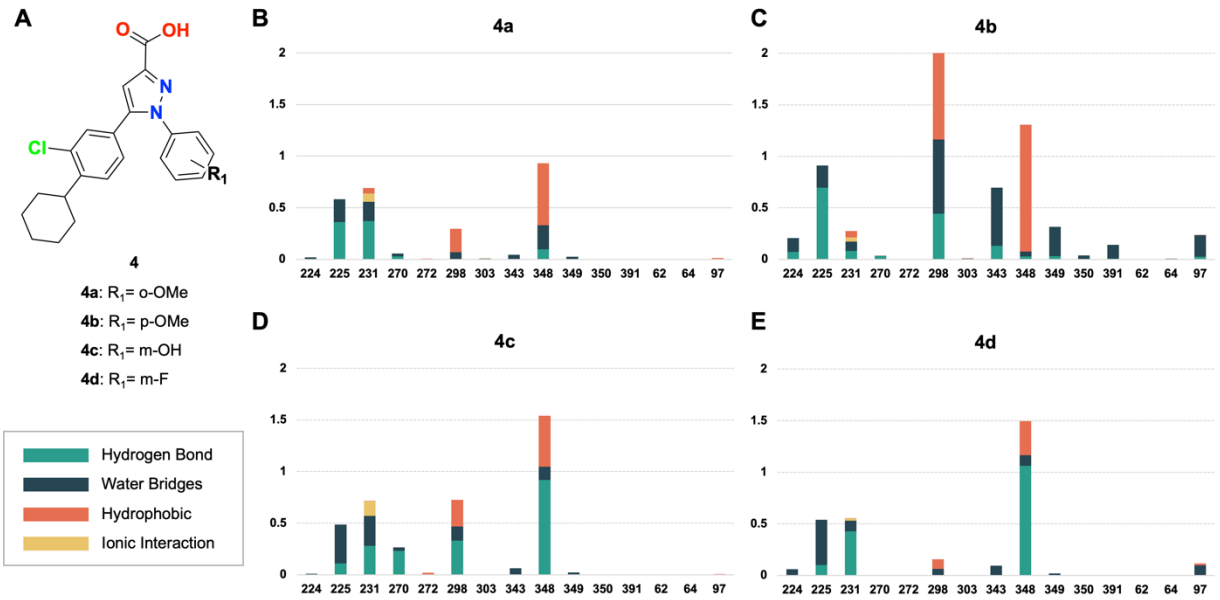

Figure 10. The binding profiles of class **4** molecules with heparanase (HPSE). The interactions are categorized in four types: hydrogen bond, water bridges, hydrophobic interaction, and ionic interaction. X axis: HPSE residue information; y axis: interaction frequency of the small molecule with the residue. (**A**) Structures of ring 2 substitution compounds **4a-4d**; (**B**) Interaction frequency of compound **4a** with HPSE; (**C**) Interaction frequency of **4b**; (**D**) Interaction frequency of **4c** with HPSE; (**E**) Interaction frequency of **4d** with HPSE.

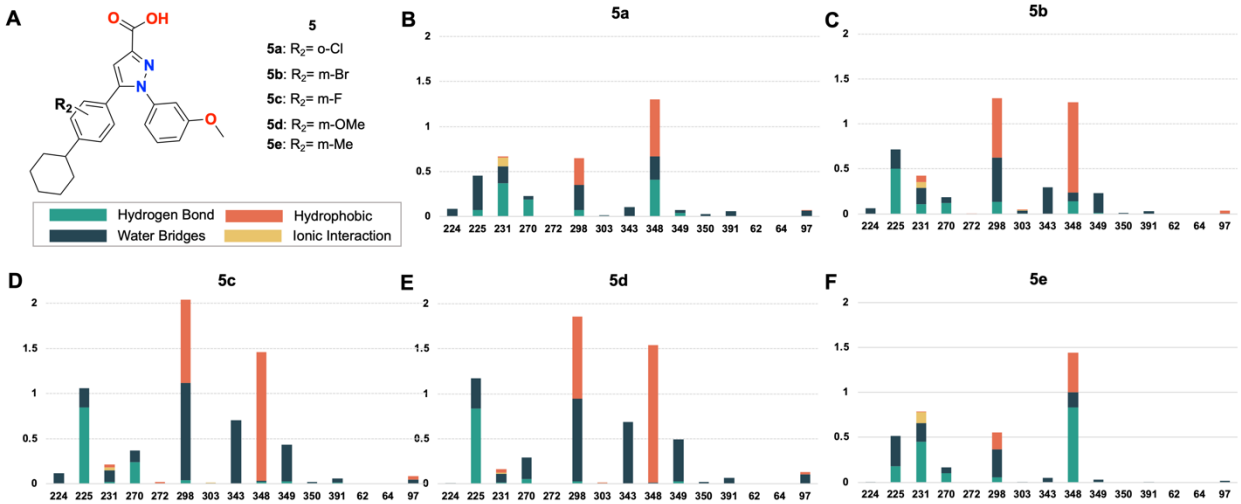

Figure 11. The binding profiles of class **5** molecules with heparanase (HPSE). The interactions are categorized in four types: hydrogen bond, water bridges, hydrophobic interaction, and ionic interaction. X axis: HPSE residue information; y axis: interaction frequency of the small molecule with the residue. (**A**) Structures of ring 3 substitution compounds **5a-5e**; (**B**) Interaction frequency of compound **5a** with HPSE; (**C**) Interaction frequency of **5b**; (**D**) Interaction frequency of **5c** with HPSE; (**E**) Interaction frequency of **5d** with HPSE; (**F**) Interaction frequency of **5e** with HPSE.

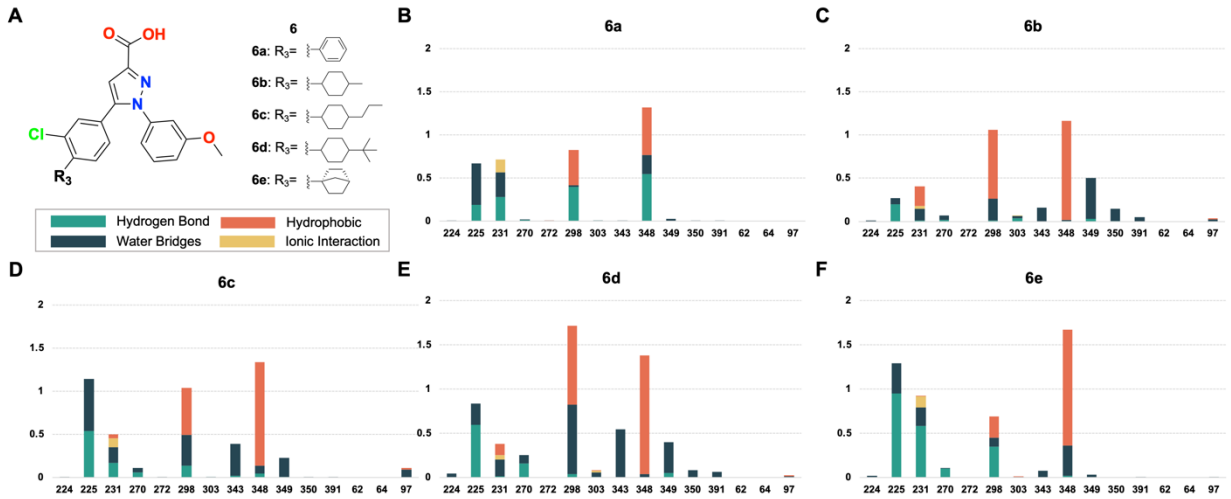

Figure 12. The binding profiles of class **6** molecules with heparanase (HPSE). The interactions are categorized in four types: hydrogen bond, water bridges, hydrophobic interaction, and ionic interaction. X axis: HPSE residue information; y axis: interaction frequency of the small molecule with the residue. (**A**) Structures of ring 4 substitution compounds **6a-6e**; (**B**) Interaction frequency of compound **6a** with HPSE; (**C**) Interaction frequency of **6b** with HPSE; (**D**) Interaction frequency of **6c** with HPSE; (**E**) Interaction frequency of **6d** with HPSE; (**F**) Interaction frequency of **6e** with HPSE.

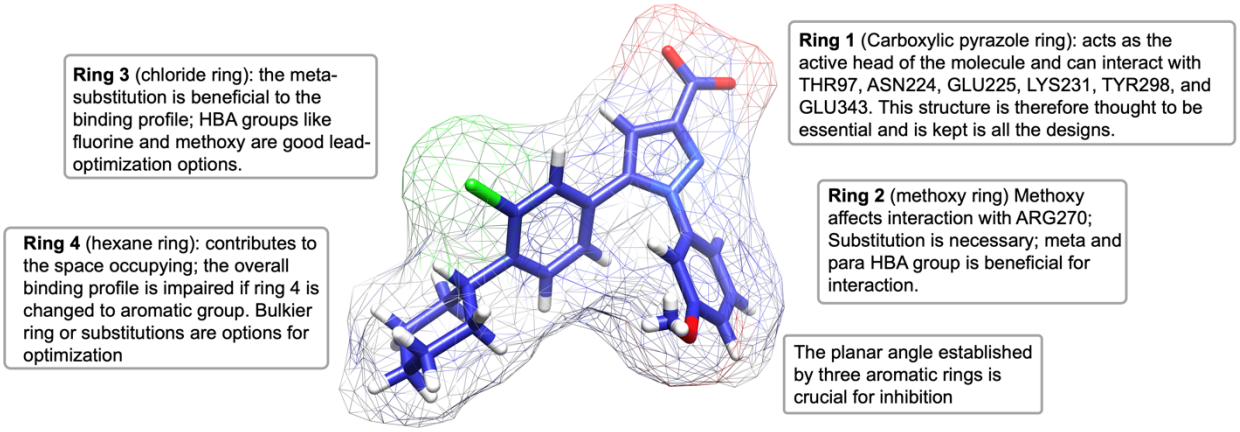

Figure 13. Summary of TC LPA5 4 structure-activity relationship (SAR) with heparanase (HPSE).

References

(1) Vlodavsky, I.; Eldor, A.; Haimovitz-Friedman, A.; Matzner, Y.; Ishai-Michaeli, R.; Lider, O.; Naparstek, Y.; Cohen, I. R.; Fuks, Z. Expression of heparanase by platelets and circulating cells of the immune system: possible involvement in diapedesis and extravasation. *Invasion Metastasis* **1992**, *12* (2), 112-127. From NLM.
(2) Hulett, M. D.; Freeman, C.; Hamdorf, B. J.; Baker, R. T.; Harris, M. J.; Parish, C. R. Cloning of mammalian heparanase, an important enzyme in tumor invasion and metastasis. *Nature Medicine* **1999**, *5* (7), 803-809. DOI: 10.1038/10525.
(3) Nardella, C.; Lahm, A.; Pallaoro, M.; Brunetti, M.; Vannini, A.; Steinkühler, C. Mechanism of activation of human heparanase investigated by protein engineering. *Biochemistry* **2004**, *43* (7), 1862-1873. DOI: 10.1021/bi030203a From NLM.
(4) Bernfield, M.; Götte, M.; Park, P. W.; Reizes, O.; Fitzgerald, M. L.; Lincecum, J.; Zako, M. Functions of Cell Surface Heparan Sulfate Proteoglycans. *Annual Review of Biochemistry* **1999**, *68* (1), 729-777. DOI: 10.1146/annurev.biochem.68.1.729 (acccessed 2023/02/15).
(5) Cole, G. J.; Halfter, W. Agrin: an extracellular matrix heparan sulfate proteoglycan involved in cell interactions and synaptogenesis. *Perspect Dev Neurobiol* **1996**, *3* (4), 359-371. From NLM.
(6) Bishop, J. R.; Schuksz, M.; Esko, J. D. Heparan sulphate proteoglycans fine-tune mammalian physiology. *Nature* **2007**, *446* (7139), 1030-1037. DOI: 10.1038/nature05817 From NLM.
(7) Peterson, S. B.; Liu, J. Unraveling the specificity of heparanase utilizing synthetic substrates. *J Biol Chem* **2010**, *285* (19), 14504-14513. DOI: 10.1074/jbc.M110.104166 From NLM.
(8) Jayatilleke, K. M.; Hulett, M. D. Heparanase and the hallmarks of cancer. *J Transl Med* **2020**, *18* (1), 453. DOI: 10.1186/s12967-020-02624-1 From NLM.
(9) Li, J. P.; Vlodavsky, I. Heparin, heparan sulfate and heparanase in inflammatory reactions. *Thromb Haemost* **2009**, *102* (5), 823-828. DOI: 10.1160/th09-02-0091 From NLM.
(10) Ilan, N.; Elkin, M.; Vlodavsky, I. Regulation, function and clinical significance of heparanase in cancer metastasis and angiogenesis. *Int J Biochem Cell Biol* **2006**, *38* (12), 2018-2039. DOI: 10.1016/j.biocel.2006.06.004 From NLM.
(11) Wang, F.; Wan, A.; Rodrigues, B. The function of heparanase in diabetes and its complications. *Can J Diabetes* **2013**, *37* (5), 332-338. DOI: 10.1016/j.jcjd.2013.05.008 From NLM.
(12) Peled, E.; Davis, M.; Axelman, E.; Norman, D.; Nadir, Y. Heparanase role in the treatment of avascular necrosis of femur head. *Thromb Res* **2013**, *131* (1), 94-98. DOI: 10.1016/j.thromres.2012.09.018 From NLM.
(13) Masola, V.; Zaza, G.; Onisto, M.; Lupo, A.; Gambaro, G. Impact of heparanase on renal fibrosis. *J Transl Med* **2015**, *13*, 181. DOI: 10.1186/s12967-015-0538-5 From NLM.

(14) Secchi, M. F.; Crescenzi, M.; Masola, V.; Russo, F. P.; Floreani, A.; Onisto, M. Heparanase and macrophage interplay in the onset of liver fibrosis. *Sci Rep* **2017**, *7* (1), 14956. DOI: 10.1038/s41598-017-14946-0 From NLM.
(15) García, B.; Martín, C.; García-Suárez, O.; Muñiz-Alonso, B.; Ordiales, H.; Fernández-Menéndez, S.; Santos-Juanes, J.; Lorente-Gea, L.; Castañón, S.; Vicente-Etxenausia, I.; et al. Upregulated Expression of Heparanase and Heparanase 2 in the Brains of Alzheimer's Disease. *J Alzheimers Dis* **2017**, *58* (1), 185-192. DOI: 10.3233/jad-161298 From NLM.
(16) Coombe, D. R.; Gandhi, N. S. Heparanase: A Challenging Cancer Drug Target. *Frontiers in Oncology* **2019**, *9*, Review. DOI: 10.3389/fonc.2019.01316.
(17) Fairbanks, M. B.; Mildner, A. M.; Leone, J. W.; Cavey, G. S.; Mathews, W. R.; Drong, R. F.; Slightom, J. L.; Bienkowski, M. J.; Smith, C. W.; Bannow, C. A.; et al. Processing of the human heparanase precursor and evidence that the active enzyme is a heterodimer. *J Biol Chem* **1999**, *274* (42), 29587-29590. DOI: 10.1074/jbc.274.42.29587 From NLM.
(18) Hulett, M. D.; Hornby, J. R.; Ohms, S. J.; Zuegg, J.; Freeman, C.; Gready, J. E.; Parish, C. R. Identification of Active-Site Residues of the Pro-Metastatic Endoglycosidase Heparanase. *Biochemistry* **2000**, *39* (51), 15659-15667. DOI: 10.1021/bi002080p.
(19) Kudchadkar, R.; Gonzalez, R.; Lewis, K. D. PI-88: a novel inhibitor of angiogenesis. *Expert Opin Investig Drugs* **2008**, *17* (11), 1769-1776. DOI: 10.1517/13543784.17.11.1769 From NLM.
(20) Ferro, V.; Liu, L.; Johnstone, K. D.; Wimmer, N.; Karoli, T.; Handley, P.; Rowley, J.; Dredge, K.; Li, C. P.; Hammond, E.; et al. Discovery of PG545: a highly potent and simultaneous inhibitor of angiogenesis, tumor growth, and metastasis. *J Med Chem* **2012**, *55* (8), 3804-3813. DOI: 10.1021/jm201708h From NLM.
(21) Ritchie, J. P.; Ramani, V. C.; Ren, Y.; Naggi, A.; Torri, G.; Casu, B.; Penco, S.; Pisano, C.; Carminati, P.; Tortoreto, M.; et al. SST0001, a chemically modified heparin, inhibits myeloma growth and angiogenesis via disruption of the heparanase/syndecan-1 axis. *Clin Cancer Res* **2011**, *17* (6), 1382-1393. DOI: 10.1158/1078-0432.Ccr-10-2476 From NLM.
(22) Zhou, H.; Roy, S.; Cochran, E.; Zouaoui, R.; Chu, C. L.; Duffner, J.; Zhao, G.; Smith, S.; Galcheva-Gargova, Z.; Karlgren, J.; et al. M402, a novel heparan sulfate mimetic, targets multiple pathways implicated in tumor progression and metastasis. *PLoS One* **2011**, *6* (6), e21106. DOI: 10.1371/journal.pone.0021106 From NLM.
(23) Abaterusso, C.; Gambaro, G. The role of glycosaminoglycans and sulodexide in the treatment of diabetic nephropathy. *Treat Endocrinol* **2006**, *5* (4), 211-222. DOI: 10.2165/00024677-200605040-00002 From NLM.
(24) Courtney, S. M.; Hay, P. A.; Buck, R. T.; Colville, C. S.; Porter, D. W.; Scopes, D. I.; Pollard, F. C.; Page, M. J.; Bennett, J. M.; Hircock, M. L.; et al. 2,3-Dihydro-1,3-dioxo-1H-isoindole-5-carboxylic acid derivatives: a novel class of small molecule heparanase inhibitors. *Bioorg Med Chem Lett* **2004**, *14* (12), 3269-3273. DOI: 10.1016/j.bmcl.2004.03.086 From NLM.
(25) Courtney, S. M.; Hay, P. A.; Buck, R. T.; Colville, C. S.; Phillips, D. J.; Scopes, D. I.; Pollard, F. C.; Page, M. J.; Bennett, J. M.; Hircock, M. L.; et al. Furanyl-1,3-thiazol-2-yl and benzoxazol-5-yl acetic acid derivatives: novel classes of heparanase inhibitor.

Bioorg Med Chem Lett **2005**, *15* (9), 2295-2299. DOI: 10.1016/j.bmcl.2005.03.014 From NLM.
(26) Madia, V. N.; Messore, A.; Pescatori, L.; Saccoliti, F.; Tudino, V.; De Leo, A.; Bortolami, M.; Scipione, L.; Costi, R.; Rivara, S.; et al. Novel Benzazole Derivatives Endowed with Potent Antiheparanase Activity. *Journal of Medicinal Chemistry* **2018**, *61* (15), 6918-6936. DOI: 10.1021/acs.jmedchem.8b00908.
(27) Messore, A.; Madia, V. N.; Pescatori, L.; Saccoliti, F.; Tudino, V.; De Leo, A.; Bortolami, M.; De Vita, D.; Scipione, L.; Pepi, F.; et al. Novel Symmetrical Benzazolyl Derivatives Endowed with Potent Anti-Heparanase Activity. *Journal of Medicinal Chemistry* **2018**, *61* (23), 10834-10859. DOI: 10.1021/acs.jmedchem.8b01497.
(28) Pan, W.; Miao, H. Q.; Xu, Y. J.; Navarro, E. C.; Tonra, J. R.; Corcoran, E.; Lahiji, A.; Kussie, P.; Kiselyov, A. S.; Wong, W. C.; et al. 1-[4-(1H-Benzoimidazol-2-yl)-phenyl]-3-[4-(1H-benzoimidazol-2-yl)-phenyl]-urea derivatives as small molecule heparanase inhibitors. *Bioorg Med Chem Lett* **2006**, *16* (2), 409-412. DOI: 10.1016/j.bmcl.2005.09.069 From NLM.
(29) Xu, Y. J.; Miao, H. Q.; Pan, W.; Navarro, E. C.; Tonra, J. R.; Mitelman, S.; Camara, M. M.; Deevi, D. S.; Kiselyov, A. S.; Kussie, P.; et al. N-(4-{[4-(1H-Benzoimidazol-2-yl)-arylamino]-methyl}-phenyl)-benzamide derivatives as small molecule heparanase inhibitors. *Bioorg Med Chem Lett* **2006**, *16* (2), 404-408. DOI: 10.1016/j.bmcl.2005.09.070 From NLM.
(30) Ishida, K.; Teruya, T.; Simizu, S.; Osada, H. Exploitation of heparanase inhibitors from microbial metabolites using an efficient visual screening system. *J Antibiot (Tokyo)* **2004**, *57* (2), 136-142. DOI: 10.7164/antibiotics.57.136 From NLM.
(31) Liu, J.; Schleyer, K. A.; Bryan, T. L.; Xie, C.; Seabra, G.; Xu, Y.; Kafle, A.; Cui, C.; Wang, Y.; Yin, K.; et al. Ultrasensitive small molecule fluorogenic probe for human heparanase. *Chem Sci* **2020**, *12* (1), 239-246. DOI: 10.1039/d0sc04872k From NLM.
(32) Huang, K. S.; Holmgren, J.; Reik, L.; Lucas-McGady, D.; Roberts, J.; Liu, C. M.; Levin, W. High-throughput methods for measuring heparanase activity and screening potential antimetastatic and anti-inflammatory agents. *Anal Biochem* **2004**, *333* (2), 389-398. DOI: 10.1016/j.ab.2004.06.023 From NLM.
(33) Gozalbes, R.; Mosulén, S.; Carbajo, R. J.; Pineda-Lucena, A. Development and NMR validation of minimal pharmacophore hypotheses for the generation of fragment libraries enriched in heparanase inhibitors. *J Comput Aided Mol Des* **2009**, *23* (8), 555-569. DOI: 10.1007/s10822-009-9269-0 From NLM.
(34) Gozalbes, R.; Mosulén, S.; Ortí, L.; Rodríguez-Díaz, J.; Carbajo, R. J.; Melnyk, P.; Pineda-Lucena, A. Hit identification of novel heparanase inhibitors by structure- and ligand-based approaches. *Bioorganic & Medicinal Chemistry* **2013**, *21* (7), 1944-1951. DOI: https://doi.org/10.1016/j.bmc.2013.01.033.
(35) Parate, S.; Kumar, V.; , D.; Hong, J. C.; Lee, K. W. Computational Investigation Identified Potential Chemical Scaffolds for Heparanase as Anticancer Therapeutics. *International Journal of Molecular Sciences* **2021**, *22* (10), 5311.
(36) Pala, D.; Rivara, S.; Mor, M.; Milazzo, F. M.; Roscilli, G.; Pavoni, E.; Giannini, G. Kinetic analysis and molecular modeling of the inhibition mechanism of roneparstat (SST0001) on human heparanase. *Glycobiology* **2016**, *26* (6), 640-654. DOI: 10.1093/glycob/cww003 From NLM.

(37) Plastira, I.; Bernhart, E.; Goeritzer, M.; DeVaney, T.; Reicher, H.; Hammer, A.; Lohberger, B.; Wintersperger, A.; Zucol, B.; Graier, W. F.; et al. Lysophosphatidic acid via LPA-receptor 5/protein kinase D-dependent pathways induces a motile and pro-inflammatory microglial phenotype. *J Neuroinflammation* **2017**, *14* (1), 253. DOI: 10.1186/s12974-017-1024-1 From NLM.
(38) Kittaka, H.; Uchida, K.; Fukuta, N.; Tominaga, M. Lysophosphatidic acid-induced itch is mediated by signalling of LPA(5) receptor, phospholipase D and TRPA1/TRPV1. *J Physiol* **2017**, *595* (8), 2681-2698. DOI: 10.1113/jp273961 From NLM.
(39) Wu, L.; Viola, C. M.; Brzozowski, A. M.; Davies, G. J. Structural characterization of human heparanase reveals insights into substrate recognition. *Nat Struct Mol Biol* **2015**, *22* (12), 1016-1022. DOI: 10.1038/nsmb.3136 From NLM.
(40) de Boer, C.; Armstrong, Z.; Lit, V. A. J.; Barash, U.; Ruijgrok, G.; Boyango, I.; Weitzenberg, M. M.; Schröder, S. P.; Sarris, A. J. C.; Meeuwenoord, N. J.; et al. Mechanism-based heparanase inhibitors reduce cancer metastasis in vivo. *Proc Natl Acad Sci U S A* **2022**, *119* (31), e2203167119. DOI: 10.1073/pnas.2203167119 From NLM.
(41) Dai, X.; Yan, J.; Fu, X.; Pan, Q.; Sun, D.; Xu, Y.; Wang, J.; Nie, L.; Tong, L.; Shen, A.; et al. Aspirin Inhibits Cancer Metastasis and Angiogenesis via Targeting Heparanase. *Clin Cancer Res* **2017**, *23* (20), 6267-6278. DOI: 10.1158/1078-0432.Ccr-17-0242 From NLM.
(42) Berman, H. M.; Westbrook, J.; Feng, Z.; Gilliland, G.; Bhat, T. N.; Weissig, H.; Shindyalov, I. N.; Bourne, P. E. The Protein Data Bank. *Nucleic Acids Research* **2000**, *28* (1), 235-242. DOI: 10.1093/nar/28.1.235 (acccessed 4/27/2021).
(43) 2021-4, S. R. Protein Preparation Wizard; Epik, Schrödinger, LLC, New York, NY. *Impact, Schrödinger, LLC, New York, NY; Prime, Schrödinger, LLC, New York, NY* **2021**.
(44) 2022-3, S. R. LigPrep, Schrödinger, LLC, New York, NY. **2021**.
(45) Shelley, J. C.; Cholleti, A.; Frye, L. L.; Greenwood, J. R.; Timlin, M. R.; Uchimaya, M. Epik: a software program for pK(a) prediction and protonation state generation for drug-like molecules. *J Comput Aided Mol Des* **2007**, *21* (12), 681-691. DOI: 10.1007/s10822-007-9133-z From NLM.
(46) Friesner, R. A.; Murphy, R. B.; Repasky, M. P.; Frye, L. L.; Greenwood, J. R.; Halgren, T. A.; Sanschagrin, P. C.; Mainz, D. T. Extra Precision Glide: Docking and Scoring Incorporating a Model of Hydrophobic Enclosure for Protein−Ligand Complexes. *Journal of Medicinal Chemistry* **2006**, *49* (21), 6177-6196. DOI: 10.1021/jm051256o.
(47) 2023-1, S. R. Desmond Molecular Dynamics System, D. E. Shaw Research, New York, NY. *Maestro-Desmond Interoperability Tools, Schrödinger, New York, NY* **2021**.
(48) Lu, C.; Wu, C.; Ghoreishi, D.; Chen, W.; Wang, L.; Damm, W.; Ross, G. A.; Dahlgren, M. K.; Russell, E.; Von Bargen, C. D.; et al. OPLS4: Improving Force Field Accuracy on Challenging Regimes of Chemical Space. *J Chem Theory Comput* **2021**, *17* (7), 4291-4300. DOI: 10.1021/acs.jctc.1c00302 From NLM.